JOURNAL OF GUIDANCE, CONTROL, AND DYNAMICS
Vol. 17, No. 5, September–October 1994

Re-Entry Control to a Drag-vs-Energy Profile

Axel J. Roenneke* and Albert Markl†
University of Stuttgart, 70176 Stuttgart, Germany

We present trajectory control for a winged re-entry vehicle based on drag-vs-energy guidance. A linear control law is derived to track the drag reference guaranteeing satisfactory drag error dynamics. For the controller design, the vehicle's motion in the vertical plane is transformed into a drag state space, and the transformed system is linearized along the drag reference. Flight simulation results show that the control system operates effectively while subject to significant atmospheric variations.

Nomenclature

$A(e)$ = system matrix
$B(e)$ = control matrix
C_D = drag coefficient
C_L = lift coefficient
D = drag acceleration, normalized by G_0
e = negative total energy, normalized by mG_0R_0
$F(e)$ = feedback gain matrix
G_0 = acceleration of gravity at sea level
g = acceleration of gravity, normalized by G_0
h_s = atmosphere scale height, normalized by R_0
m = mass of vehicle
R_0 = radius of Earth
r = distance from Earth's center, normalized by R_0
S = reference area
s = horizontal range, normalized by R_0
t = flight time, normalized by $\sqrt{R_0/G_0}$
u = vertical lift-to-drag ratio, $(C_L/C_D)\cos\sigma$
v = Earth-relative speed, normalized by $\sqrt{G_0R_0}$
γ = flight-path angle
$\delta x(t)$ = state error vector
ρ = atmospheric density
σ = bank angle

Introduction

IN guided re-entry, atmospheric drag is controlled to dissipate excess energy. The objective is to deliver the vehicle to a desired destination with an energy state sufficient for approach and landing. Typically, on-board guidance systems use a nominal reference to predict the range-to-go and trajectory control to keep the predictions within satisfactory error bounds. In case of a predicted target miss, the reference is modified.[1–5]

In the U.S. Space Shuttle guidance,[5] the reference is drag vs velocity as the independent variable. Based on this reference, range is predicted through an analytic approximation. However, the prediction is best for shallow entry paths. In steep descent near the target threshold, the schedule is switched to drag vs energy to improve the accuracy of the predicted range. This concept has been very successful for missions from low-Earth orbit to California and Florida with a moderate cross-range.[6]

Re-entry flights from a space station low-Earth orbit to Europe require a large cross-range close to the performance limits of high-lift re-entry vehicles.[7] Several roll reversals to align heading, which is a typical feature of the Shuttle guidance, will not be feasible. Applied to European missions, the Shuttle ranging has not been proven to be accurate enough.[7] Simulations show that in the presence of expected parameter variations the target miss at Mach 2 may be up to 100 km.

Several new guidance laws have been suggested for European demands. One concept is to observe both position and velocity and use an analytic optimal control law to achieve zero position error at final time.[7] Another approach is to schedule total energy vs range and control both kinetic and potential energy by adjusting bank angle and angle of attack independently.[8]

The concept presented here is an extension of the Shuttle approach. In the Shuttle guidance, the drag function is constructed from pieces of parabola functions. To adjust for target dispersions, an entire trajectory segment is shifted to a new drag level. A more general approach is to model the drag function as a cubic spline over a number of break points. To achieve the required range, the drag level of each break point is determined by numerical trajectory optimization. To apply this approach consistently to all flight phases, we suggest scheduling drag vs total energy from the beginning of atmospheric entry to the terminal-area interface. Total energy is the independent variable for both guidance and trajectory control.

This method has three advantages: an accurate analytic approximation of the range to go is possible regardless of the current flight-path angle; no distinction of different trajectory segments is necessary; the terminal-area energy management interface is a natural terminal state. Path constraints, loft ceiling, thermal constraints, normal load, and dynamic pressure limits can be represented in the drag-vs-energy domain as easily as in the drag-velocity plane.

A numerical optimization method to obtain the drag reference in flight has been presented in a previous paper.[9] In this paper, a linear control law is presented that achieves local tracking of the drag-vs-energy reference and satisfactory drag error dynamics. Simulation results in this paper show that the control system operates effectively while subject to significant atmospheric variations.

Drag-vs-Energy Guidance

To develop the guidance law, the re-entry dynamics are approximated by the vehicle's translational motion over a stationary, spherical Earth. The forces acting on the vehicle are gravity and aerodynamic lift and drag. Wind disturbances are not considered. In terms of standard flight-path coordinates, the state equations in the vertical plane (containing the velocity and gravity vectors) are given by[5,10]

$$\dot{r} = v\sin\gamma \tag{1}$$

$$\dot{v} = -D - g\sin\gamma \tag{2}$$

$$v\dot{\gamma} = \left(\frac{v^2}{r} - g\right)\cos\gamma + Du \tag{3}$$

The dot indicates differentiation with respect to nondimensional time t. Input to this system is the vertical component of the lift-

Received June 23, 1993; presented as Paper 93-3790 at the AIAA Guidance, Navigation, and Control Conference, Monterey, CA, Aug. 9–11, 1993; revision received Nov. 8, 1993; accepted for publication Nov. 16, 1993.

*Research Scientist, Institute of Flight Mechanics and Control, Forst St. 86. Member AIAA.
†Research Scientist, Institute of Flight Mechanics and Control, Forst St. 86.

to-drag ratio (C_L/C_D), which is controlled by the air-path bank angle σ:

$$u = \frac{C_L}{C_D}\cos\sigma \tag{4}$$

The normalized drag acceleration D represents an output of the system given by

$$D = \frac{\rho}{(m/S)R_0}\frac{v^2}{2}C_D \tag{5}$$

where ρ is the atmospheric density and m/S is the ballistic load.

As an additional state variable, we define the negative total energy

$$e \equiv \frac{1}{r} - \frac{v^2}{2} \tag{6}$$

From circular orbit to landing, the value of e goes from approximately 0.5 to 1. Substituting Eqs. (1) and (2) and assuming a Newtonian gravity law ($g = 1/r^2$), the energy rate of change can be expressed as the product of drag and velocity:

$$\dot{e} = Dv \tag{7}$$

This expression holds for any value of the flight-path angle.

The vehicle's horizontal range s is determined by the equation of motion in the horizontal plane:

$$\dot{s} = v\cos\gamma \tag{8}$$

Substituting Eq. (7), the change of range with respect to total energy is given by

$$\frac{\partial s}{\partial e} = \frac{\cos\gamma}{D} \tag{9}$$

Approximating $\cos\gamma$ with unity, range can be estimated by the integral of drag vs total energy:

$$s \approx \int_{e_i}^{e_f} \frac{1}{D}\,de \tag{10}$$

This expression is sufficiently accurate over the entire entry regime including the final arc when γ is smaller than -5 deg. By scheduling drag vs energy, a single guidance reference is provided from the beginning of the sensible atmosphere to the terminal-area energy management interface. Unlike the Shuttle guidance, there is no need to switch the reference representation in flight.

Optimal Trajectory

To demonstrate the guidance problem, we have chosen a specific mission from low-Earth orbit (500 km altitude, 28.5 deg inclination) to Istres in Southern France.[11] The atmospheric entry interface is at an altitude of 79 km; the initial entry states are listed in Table 1. The ground track and the corresponding reference drag schedule are shown in Fig. 1.

In the optimization, the drag profile is defined as a cubic spline with 14 break points, 12 of them optimized. In Fig. 1, the optimal drag values are labeled with stars; the upper and lower bounds are marked with circles. The values of the first and the second break points are fixed to accommodate a prescribed flare maneuver.[9] Additional parameters to be optimized are the time of deorbit, the deorbit impulse, and the right ascension of the ascending node of the transfer orbit.

Table 1 Initial conditions of atmospheric entry

State	Nominal value
Altitude, km	79.2
Earth-relative velocity, m/s	7492
Flight-path angle, deg	−0.46
Heading clockwise from north, deg	29.1
West longitude, deg	39.2
North latitude, deg	13.5

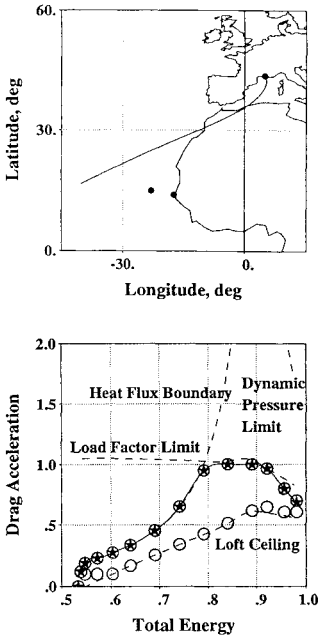

Fig. 1 Nominal trajectory to Istres, France, and corresponding drag schedule.

The reference trajectory is generated by sequential quadratic optimization subject to the translational equations of motion over a rotating, spherical Earth.[9,12] The cost criterion is the accumulated heat load at the stagnation region. Path constraints of the optimization are a maximum nose-cap temperature of 1770 K, a load factor of 1.65, a dynamic pressure boundary of 14,400 Pa, as well as a "no-skip" restriction. These bounds are well within design limits of winged re-entry vehicles.[9] In Fig. 1, the path constraints are plotted with dashed lines. As an additional terminal restriction, the heading alignment circle must be approached from east.

Transformation into Drag State Space

Equations (1–3) and (7) represent a system of four state equations. The output, given by Eqs. (5) and (6), is to follow a nominal trajectory. Instead of solving this tracking problem, it is convenient to transform Eqs. (1–3) to a drag state space, as shown in the following. In the transformed system, the drag-vs-energy trajectory represents a state-variable reference, rather than a reference of the output. The input of the system remains the same. In this fashion, the problem reduces to regulating the drag system to a desired set point.

Approximating the atmospheric density by an exponential function of the altitude, the density rate of change is given by

$$\dot{\rho} = -\rho\frac{\dot{r}}{h_s} \tag{11}$$

where h_s is a constant scale height. The drag dynamics follow from differentiating Eq. (5) and substituting Eq. (11):

$$\frac{\dot{D}}{D} = -\frac{\dot{r}}{h_s} + \frac{2\dot{v}}{v} \tag{12}$$

$$\frac{\ddot{D}}{D} = \frac{\dot{D}^2}{D^2} - \frac{\ddot{r}}{h_s} + \frac{2\ddot{v}}{v} - \frac{2\dot{v}^2}{v^2} \tag{13}$$

Here C_D is assumed constant. Differentiating Eq. (1), substituting Eqs. (3) and (12), and approximating $\cos\gamma \approx 1$, the vertical acceleration can be expressed as a linear function of the control:

$$\begin{aligned}\ddot{r} &= \frac{\dot{v}}{v}\dot{r} + v\dot{\gamma} \\ &= \frac{\dot{v}}{v}h_s\left(\frac{2\dot{v}}{v} - \frac{\dot{D}}{D}\right) + \left(\frac{v^2}{r} - g\right) + Du\end{aligned} \tag{14}$$

Combining Eqs. (1), (2), and (12), the velocity derivatives can be written in terms of drag as well:

$$\dot{v} = \left(-D + gh_s \frac{\dot{D}}{Dv}\right)\left(1 + \frac{2gh_s}{v^2}\right)^{-1} \tag{15}$$

$$\ddot{v} = -\dot{D} - \frac{g}{v}\left(\frac{v^2}{r} - g\right) - \frac{Dg}{v}u \tag{16}$$

The value of $|\dot{g}\sin\gamma|$ is neglected. Defining a set of drag state variables,

$$[x_1 \quad x_2 \quad x_3 \quad x_4]^T = [D \quad \dot{D} \quad v \quad e]^T \tag{17}$$

the drag state-space system is given by Eqs. (13) and (15):

$$\dot{x_1} = x_2 \tag{18}$$

$$\dot{x_2} = \frac{x_2^2}{x_1} - \frac{4x_1\dot{v}^2}{x_3^2} + \frac{x_2\dot{v}}{x_3} - \frac{2x_1x_2}{x_3} - x_1\left(\frac{2g}{x_3^2} + \frac{1}{h_s}\right)\left(\frac{x_3^2}{r} - g\right) - x_1\left(\frac{2x_1g}{x_3^2} + \frac{x_1}{h_s}\right)u \tag{19}$$

$$\dot{x_3} = \left(-x_1 + gh_s\frac{x_2}{x_1x_3}\right)\left(1 + \frac{2gh_s}{x_3^2}\right)^{-1} \tag{20}$$

$$\dot{x_4} = x_1x_3 \tag{21}$$

The expression for $\dot{v}$ is given by the right-hand side of Eq. (20) and r and g are approximated by constant mean values. Equation (21) is identical to Eq. (7) and is decoupled from the other state equations.

A similar drag transformation is used in the derivation of the Shuttle guidance[5] and is also suggested in Ref. 13. There, however, the denominator term in Eq. (15) is set equal to 1, neglecting the fraction $2gh_s/v^2$. This approximation does not hold below Mach 5.

Drag Reference

Given the optimal drag-vs-energy profile, all nominal drag state values are derived as functions of energy with the above transformation relationships. These reference values represent the nominal state trajectories the control system is to maintain.

From the reference drag $D_R(e)$, the reference velocity $v_R(e)$ is obtained by solving Eqs. (5) and (6) simultaneously for nominal aerodynamics and standard atmosphere data. Using Eq. (7), the corresponding drag derivatives are estimated at

$$\dot{D}_R = D'Dv \tag{22}$$

$$\ddot{D}_R = D''D^2v^2 + (D')^2Dv^2 + D'D\dot{v} \tag{23}$$

where the dash indicates partial differentiation with respect to e. The expression for $\dot{v}$ is given by Eq. (15), approximating g by a constant mean. The input corresponding to the drag reference is obtained by inverting the drag dynamics

$$u_R = \left[\frac{\dot{D}^2}{D^2} - \frac{\ddot{D}}{D} - \frac{4\dot{v}^2}{v^2} + \frac{\dot{D}\dot{v}}{Dv} - \frac{2\dot{D}}{v} - \left(\frac{2g}{v^2} + \frac{1}{h_s}\right)\left(\frac{v^2}{r} - g\right)\right]\left(\frac{2Dg}{v^2} + \frac{D}{h_s}\right)^{-1} \tag{24}$$

and substituting the reference drag derivatives $\dot{D}_R$ and $\ddot{D}_R$ from above.

Trajectory Control

The transformation from flight-path states to drag states is based on model assumptions that do not exactly equal reality. The nominal control input at a given reference is approximated by inverting these transformed dynamics. Consequently, the in-flight drag trajectory of the nominal input will not perfectly match the reference. Without trajectory control, the drag error dynamics are governed by the eigenmodes of the drag system. For an acceptable guidance performance, this may not be sufficient. Feedback stabilization is necessary to shape the drag error time response as desired.

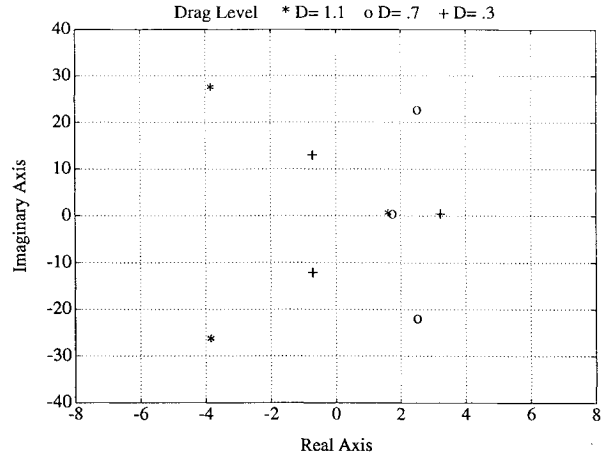

Fig. 2 Pole locations of uncontrolled drag system.

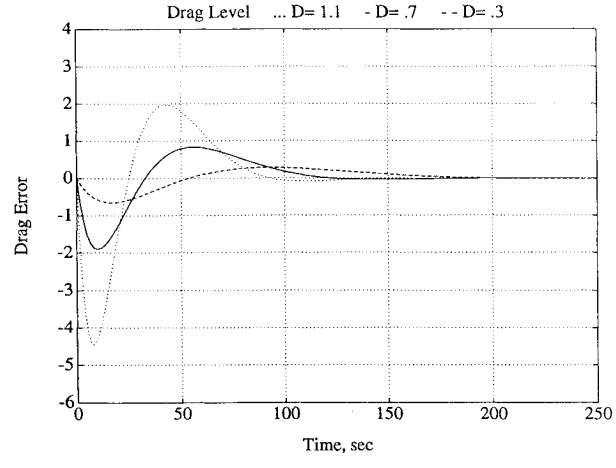

Fig. 3 Drag error impulse response of linear control system at different drag levels.

The controller is designed for a linear system of the drag state error with respect to the reference $\delta x = [D - D_R, \dot{D} - \dot{D}_R, v - v_R]^T$ and the control error $\delta u = u - u_R$. For small deviations, a linear system can be defined as

$$\delta\dot{x} = A_R\,\delta x + B_R\,\delta u \tag{25}$$

The system and control matrices A and B are functions of the reference and are approximated at discrete energy values e_k by constant matrices $A(e_k)$ and $B(e_k)$, which are obtained numerically.

Figure 2 shows the eigenvalue locations of the uncontrolled system at different drag levels. In this plot, the frequency is normalized by $\sqrt{G_0/R_0}$. A modal analysis shows that the single real pole in the right half-plane corresponds to the velocity state, whereas the conjugate pair corresponds to the second-order drag dynamics. The imaginary poles are unstable at intermediate drag values and are stable at low- and high-drag conditions; the damping ratio is not sufficient.

To shape the drag error dynamics, a linear control law is suggested of the form

$$\delta u = -F(e_k)\,\delta x \tag{26}$$

with constant feedback gains $F(e_k)$ at 20 discrete energy values. The chosen feedback gains guarantee time constants between 200 and 90 s, depending on the drag level. The poles are placed in a Butterworth configuration. In Fig. 3 the impulse responses of the controlled drag system are plotted at different drag levels. This control law is sufficient to achieve local drag tracking.

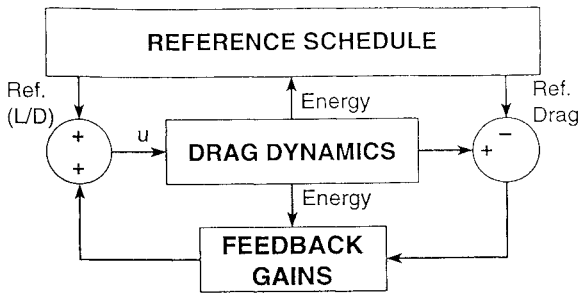

Fig. 4 Trajectory control system block diagram.

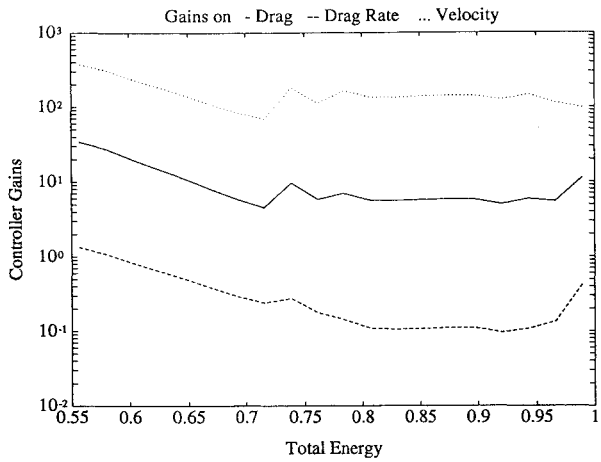

Fig. 5 Controller gains vs energy.

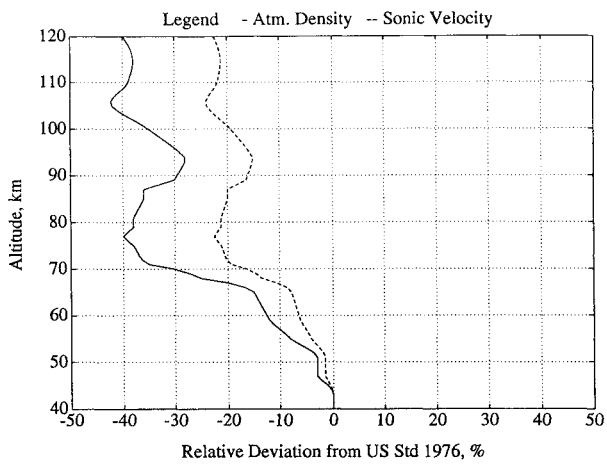

Fig. 6 North latitude atmospheric data measured on Shuttle entry flights.

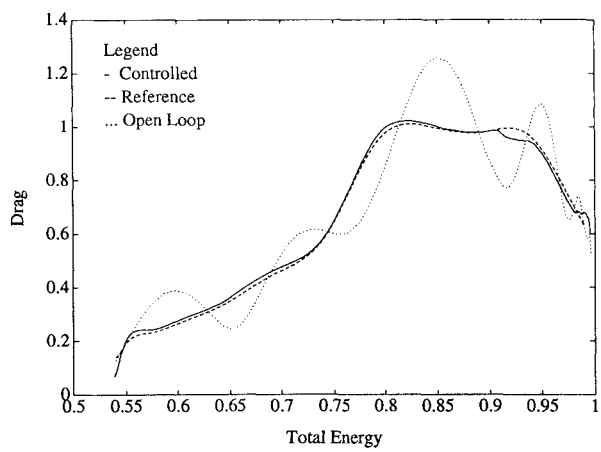

Fig. 7 Drag-vs-energy trajectory of controlled re-entry flight subject to off-nominal atmospheric data.

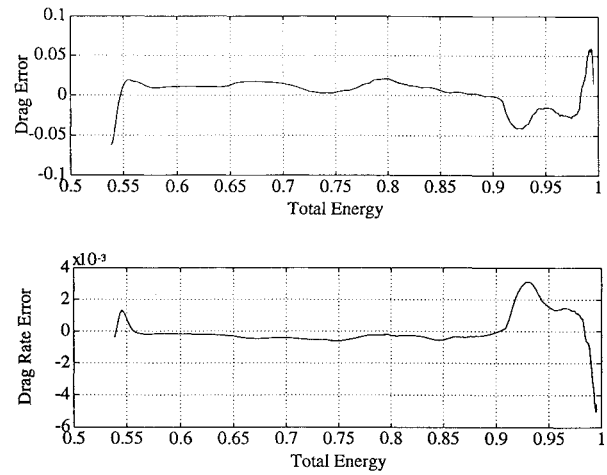

Fig. 8 Drag error (top) and drag rate error (bottom) vs energy.

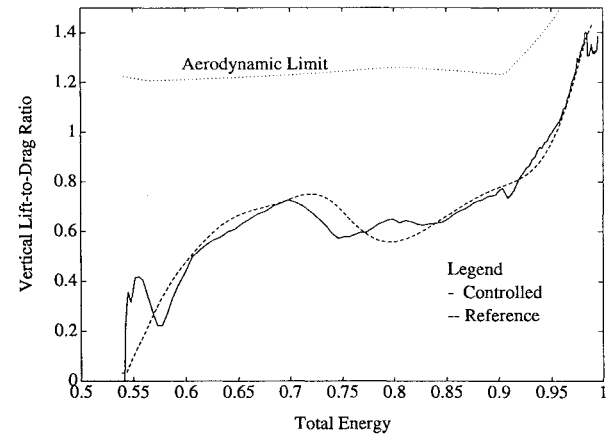

Fig. 9 Vertical lift-to-drag ratio vs energy.

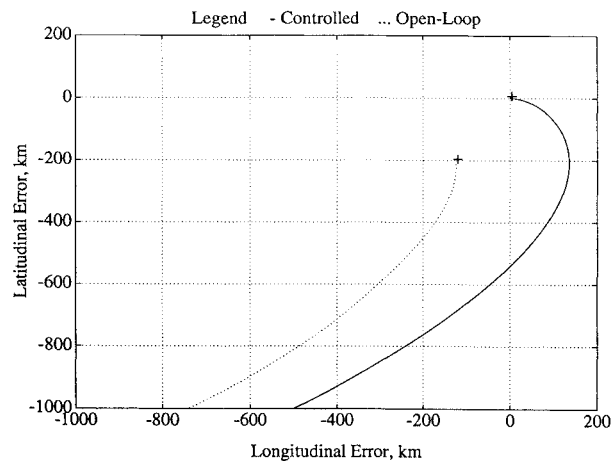

Fig. 10 Ground track and final location at Mach 2 relative to target.

Controller Performance

To evaluate the controller performance, the re-entry trajectory is simulated by the translational motion of a rigid body. The equations of motion are derived for a rotating, spherical Earth without wind. The vehicle's aerodynamic data correspond to the Hermes vehicle configuration[9] with a ballistic load m/S of approximately 220 kg/m^2. The aerodynamic coefficients are functions of the Mach number only, since the vehicle's angle of attack is controlled to a Mach-dependent schedule.

A block-diagram schematic of the simulated control system is shown in Fig. 4. The drag dynamics are given by the equations of

motion in the flight-path system with output equations (5) and (12) for drag and drag rate. The reference and the feedback gains are scheduled vs energy. During the simulation, the energy reference must be transformed into the corresponding value for a stationary Earth, since the controller design is based on the stationary Earth equations. The simulated gain schedule is plotted in Fig. 5.

For nominal flight conditions, atmospheric data are taken from the U.S. Standard Atmosphere 1976.[14] During controller simulation, the atmospheric density and sonic velocity are changed to data measured on Space Shuttle entry flights with north latitude.[15] This density profile deviates up to 40% from the Standard Atmosphere between 120 and 40 km altitude, as shown in Fig. 6. To model drag measurement errors, the drag rate of change is approximated by Eq. (12) with h_s being constant.

The simulated drag trajectory is shown in Fig. 7. In the presence of atmospheric disturbances, the uncontrolled system exhibits large oscillations. On the other hand, the controlled system follows the reference with sufficient accuracy. The drag error (see Fig. 8) is controlled to a margin of $\pm.05$ g. The necessary control effort is very close to the nominal and at no time near the aerodynamic limit (see Fig. 9). The ground track of these trajectories is shown in Fig. 10. In the uncontrolled case, the drag oscillations reduce the vehicle's kinetic energy earlier than desired. At Mach 2, when the simulation is terminated, the uncontrolled vehicle is more than 200 km short of the desired landing site, whereas the controlled vehicle is precisely on target. The controlled vehicle also approaches the landing site from east, satisfying the terminal heading constraint.

Conclusions and Future Work

This paper presents re-entry control by tracking drag vs energy. A linear control law is designed to shape the drag error response and to follow the nominal drag reference. The control system is simulated in re-entry flights from low-Earth orbit to France, which require a significant cross-range. Simulations demonstrate that the control law effectively compensates for large atmospheric disturbances, and induced landing dispersions are eliminated.

We plan to combine the presented control law with an on-board numerical trajectory optimization method. For a refined controller design, measurement errors and state estimation will be included.

References

[1]Wingrove, R. C., "A Survey of Atmosphere Re-Entry Guidance and Control Methods," *AIAA Journal*, Vol. 1, No. 9, 1963, pp. 2019–2029.

[2]Box, D. M., Harpold, J. C., Paddock, S. G., Armstrong, N. A., and Hamby, W. H., "Controlled Re-Entry," Gemini Summary Conference, NASA SP-138, Feb. 1967, pp. 159–166.

[3]National Aeronautics and Space Administration, "Guidance and Navigation for Entry Vehicles," NASA Space Vehicle Design Criteria, NASA SP-8015, Nov. 1968.

[4]Graves, C. A., and Harpold, J. C., "Apollo Experience Report—Mission Planning for Apollo Entry," NASA TN D-6725, 1972.

[5]Harpold, J. C., and Graves, C. A., "Shuttle Entry Guidance," *Journal of the Astronautical Sciences*, Vol. 26, No. 3, 1979, pp. 239–268.

[6]Harpold, J. C., and Gravert, D. E., "Space Shuttle Entry Guidance Performance Results," *Journal of Guidance, Control, and Dynamics*, Vol. 6, No. 6, 1983, pp. 442–447.

[7]Jouhaud, F., "Closed Loop Reentry Guidance Law of a Space Plane," 42nd International Astronautical Federation Congress (Montreal, Canada), Oct. 1991.

[8]Buhl, W., "Guidance and Control for Reentry Vehicles," *Proceedings of the First ESA International Conference on Spacecraft Guidance, Navigation, and Control Systems*, Noordwijk, The Netherlands, ESA SP-323, Aug. 1991, pp. 543–553.

[9]Jänsch, C., and Markl, A., "Trajectory Optimization and Guidance for a Hermes-Type Reentry Vehicle," *Proceedings of the 1991 AIAA Guidance, Navigation, and Control Conference* (New Orleans, LA), AIAA, Washington, DC,1991, pp. 543–553 (AIAA Paper 91-2659).

[10]Vinh, N. X., *Optimal Trajectories in Atmospheric Flight*, Elsevier, New York, 1981.

[11]Roenneke, A. J., and Markl, A., "Reentry Control to a Drag vs Energy Profile," *Proceedings of the 1993 AIAA Guidance, Navigation, and Control Conference* (Monterey, CA), AIAA, Washington, DC, 1993, pp. 837–844 (AIAA Paper 93-3790).

[12]Jänsch, C., Schnepper, K., Well, K. H., and Kraft, D., "Survey on Trajectory Optimization Methods," Advanced Launcher Trajectory Optimization Software, Technical Rept. 1, ESA European Space and Technology Center, Noordwijk, The Netherlands, Contract 8046/88/NL/MAC, March 1990.

[13]Mease, K. D., and Kremer, J. P., "Shuttle Entry Guidance Revisited," AIAA Paper 92-4450, Aug. 1992.

[14]U.S. National Oceanic and Atmospheric Administration, *U.S. Standard Atmosphere 1976*, U.S. Government Printing Office, Washington, DC, NOAA-S/T 76-1562, 1976.

[15]Gamble, J. D., and Findlay, J. T., "Shuttle-Derived Densities in the Middle Atmosphere," AIAA Paper 88-4352, 1988.